Available online at www.sciencedirect.com
ScienceDirect
C. R. Physique 8 (2007) 717–736
COMPTES RENDUS PHYSIQUE
http://france.elsevier.com/direct/COMREN/

Neutron scattering/Diffusion de neutrons

Modern quantum magnetism by means of neutron scattering

Béatrice Grenier [a,*], Timothy Ziman [b]

[a] *Université Joseph-Fourier Grenoble I and CEA-Grenoble, DRFMC/SPSMS/Laboratoire magnétisme et diffraction neutronique, 38054 Grenoble cedex 9, France*

[b] *CNRS and Institut Laue-Langevin, 6, rue Jules Horowitz, BP 156, 38042 Grenoble cedex 9, France*

Available online 19 November 2007

Abstract

We review a selection of recent applications of neutron scattering to the field of quantum magnetism. We focus on systems where, because of quantum fluctuations enhanced by frustration and low dimension, there is no long range magnetic order in the ground state. We select two examples that we treat in more depth to show how neutron studies, in conjunction with the results of other experimental techniques, can give new insights. The first is the case of the spin ladder NaV_2O_5, where the origin of the spin gap at low temperature is now understood in detail. Apparent contradictions between quantitative measures of the charge order from neutron inelastic scattering, resonant X-ray scattering and NMR have been resolved giving interesting insights into the correlations. The second case is that of spin dimer system $Cs_3Cr_2X_9$ ($X = \mathrm{Br}, \mathrm{Cl}$), undergoing transitions to field induced transverse magnetic order. The Br compound is attractive as the critical fields are sufficiently low that a complete study, in different field directions, is possible. In addition, it is noteworthy in that the magnon that softens and condenses is incommensurable with the lattice. The common description in terms of Bose–Einstein condensation must be extended to include a continuous degeneracy and single ion anisotropy, and conclusions can be drawn by comparison with the Cl compound. ***To cite this article: B. Grenier, T. Ziman, C. R. Physique 8 (2007).***

Résumé

Étude du magnétisme quantique moderne par diffusion des neutrons. Nous passons en revue une sélection des applications récentes de la diffusion neutronique dans le domaine du magnétisme quantique. Nous nous concentrons sur des systèmes où, du fait des fluctuations quantiques amplifiées par la frustration et la basse dimension, l'état fondamental ne présente pas d'ordre magnétique à longue portée. Nous détaillons deux exemples afin de montrer comment les études neutroniques, conjointement à d'autres techniques expérimentales, peuvent apporter de nouvelles connaissances. Le premier est l'échelle de spin NaV_2O_5 où l'origine du gap de spin à basse température est maintenant comprise en détail. Les contradictions apparentes entre les mesures quantitatives de l'ordre de charge par diffusion inélastique des neutrons, diffraction résonante des rayons X et RMN ont été résolues, conduisant à des résultats intéressants sur les corrélations. Le second exemple est le système à dimères de spins $Cs_3Cr_2X_9$ ($X = \mathrm{Br}, \mathrm{Cl}$) qui subit des transitions vers un ordre magnétique transverse induit sous champ. Le composé au Br est attrayant pour ses faibles valeurs de champs critiques, permettant ainsi une étude complète, avec différentes directions du champ. Il est de plus remarquable que le magnon qui s'amollit et se condense est incommensurable avec le réseau. La description commune en terme de condensation de Bose–Einstein doit être étendue pour inclure la dégénérescence continue et l'anisotropie à un ion, et des conclusions peuvent être tirées par comparaison avec le composé au Cl. ***Pour citer cet article : B. Grenier, T. Ziman, C. R. Physique 8 (2007).***

* Corresponding author.
E-mail addresses: grenier@ill.eu (B. Grenier), ziman@ill.eu (T. Ziman).

1631-0705/$ – see front matter
doi:10.1016/j.crhy.2007.09.016

Keywords: Low-dimensional magnetism; Field-induced magnetic ordering; Spin excitations; Magnetic neutron scattering

Mots-clés : Magnétisme à basse dimension ; Ordre magnétique induit sous champ ; Excitations de spin ; Diffusion magnétique des neutrons

1. Introduction: quantum magnetism and contribution of neutron scattering

We review a small selection of current work on quantum magnets where the use of neutrons has made apparent concepts that were barely known thirty years ago. To measure the progress we can compare current results with those reviewed extensively by Steiner, Villain and Windsor [1] in 1976. We will emphasize systems which have in common that, while they have well developed local magnetic moments, they have non-magnetic ground states, at least in zero field. The moments do not simply order as ferromagnets or antiferromagnets in zero field since quantum fluctuations are enhanced by the low spatial dimension and/or frustration, i.e. competition of different possible magnetic orders. Such systems have generated enormous amount of attention for several reasons: (i) The general interest in quantum fluctuations and quantum critical points. This developed particularly in the 1980s, driven by the much better understanding of the role of fluctuations in classical phase transitions. Experimentally this was through the observation of critical scattering and theoretically from the application of field theoretical methods and renormalization group calculations. It was natural to look at the same methods for quantum phase transitions. (ii) The discovery of high T_c superconductivity in copper oxide materials in the late 1980s gave a boost to the subject because of the importance of understanding the interplay of magnetic fluctuations and superconductivity, especially in low dimension. (iii) The availability of single crystals of materials which closely approximate some of model systems. In many crystals the magnetic moments are well described by quasi-one (or -two) dimensional Hamiltonians. If we compare the situation now to that when the review article [1] was written, to look at one dimensional Heisenberg systems, for example, there are several new examples that are more isotropic in spin space (more accurately Heisenberg) and less three-dimensional (weaker interactions between adjacent chains). For example, compare NENP [2] to $CsNiCl_3$ [3] for $s = 1$. The Hamiltonians for the systems we will discuss can be written as

$$\mathcal{H} = \sum_{i,j} J_{i,j}\, \vec{S}_i \cdot \vec{S}_j + \sum_i D_i \left(S_i^{\alpha}\right)^2 + \sum_{i,j} \vec{M}_{i,j} \cdot (\vec{S}_i \times \vec{S}_j) \tag{1}$$

where the summations i, j are determined by the geometry of the lattice, $J_{i,j}$ are the strengths of isotropic Heisenberg interactions between spins $\vec{S}_i$ and $\vec{S}_j$, D_i is a single-ion anisotropy with respect to some axis α and $\vec{M}_{i,j}$ is the vector determining possible Dzyaloshinskii–Moriya interactions. Other anisotropies occur (in the exchange term, higher order single-ion anisotropies, ...) but will not appear in the examples we discuss.

This introduction intends to give a brief review about quantum magnetic systems, starting from low-dimensional systems and going to higher dimension, with both model and real systems (including anisotropy, frustration, and other degrees of freedom such as charge, structure), and then focussing on field-induced magnetism in gapped systems. The central role of neutron scattering will be illustrated with two materials treated in detail: Section 2 will present a study by neutron inelastic scattering performed in the spin-ladder compound NaV_2O_5, and will show how the complementarity between neutrons and X-rays played a crucial role in the understanding of this compound. Section 3 will be devoted to combined neutron elastic and inelastic scattering studies of the field-induced magnetic ordering (FIMO) phase of the spin 3/2 dimer system $Cs_3Cr_2X_9$ (X = Br, Cl). It will illustrate how useful it is to study simultaneously the magnetic structure and the spin dynamics.

1.1. Model systems

Probably the most studied model systems have been those which are approximately one-dimensional (1D), i.e. where the summation i, j in Eq. (1) is between neighbors along a single direction in space. They are particularly attractive as there is a wealth of information from a theoretical point of view and concepts which are far from that of classical mean field. For example, theorists have the tools of low dimensional field theories originating in Luttinger field theories in the 1950s and developed in the 1970s and 80s in what is now known as 'fermionization' and 'bosonization' methods [4]. Such continuum theories are complemented by exact results of integrable models obtained

by methods known as Bethe Ansatz methods [5] which continue to yield more exact information on special Hamiltonians. Neither low dimensional continuum field theory nor the methods of integrable systems are perturbative. Thus phenomena can, and do, appear that are very different from those seen in more classical stable magnetic structures where standard Dyson–Maleev spin wave theory reduces the dynamics to that of a gas of weakly interacting harmonic oscillators. Originally the low dimension meant that in the experimental field of magnetism the non-perturbative results had little direct relevance, but thanks to the study of new materials with, for example, loosely coupled chains of magnetic ions, relatively obscure concepts such as conformal field theories, quantum critical points can be seen to be essential to understanding experimental systems. Nowadays there is, of course, more direct fabrication of artificial structures which are literally low dimensional, so in principle one can study a single chain magnet rather than a crystal of weakly coupled chains. Here neutrons are of less obvious application, simply because scattering from a single chain is too weak, but the conclusions of neutron studies are directly applicable.

1.2. 1D systems

The argument which probably first convinced the wider community of the qualitative importance of quantum fluctuations in low dimensions was that of Haldane [6] who predicted that the quantum Heisenberg model (first term of Eq. (1)) in one dimension would show a gap to excitations, between the singlet ground state and the first excited triplet state, in the absence of any spin anisotropy, provided that the spins were integer (e.g. spin 1) rather than half-integer. For those used to three dimensional magnets this seemed surprising: The standard argument is that a simple two sublattice Heisenberg antiferromagnet orders at low temperature with a sublattice magnetization in some arbitrary direction. Since the direction of the sublattice can be *continuously* changed without affecting the energy, there must be infinitesimal changes, linear spin waves or magnons whose frequencies vanish at the wave vector associated with the alternation. This argument is valid beyond spin wave theory and the vanishing spin wave is known as a Goldstone mode. If we observe a gap in a three dimensional magnetic system we attribute it to anisotropy. Haldane concluded that this is incorrect in one dimension: Gaps may be generated even for perfect spin isotropy. He argued that in one dimension, the Goldstone mode associated with a classical breaking of symmetry in the ground state acquired a gap because quantum fluctuations suppress the symmetry breaking. This was despite the fact that for spin $1/2$, where one might expect stronger fluctuations, exact solutions [7] had proved that there are gapless excitations even though there is no symmetry breaking: The sublattice magnetization vector processes in all directions. The subtlety of the argument, based on a large spin expansion, was that it predicted a gap for the integer case, but no gap in the half-integer case. This introduced the concept of topological terms into the non-linear sigma-model describing spin dynamics. For spin $1/2$ chains, the gapless triplets of spin 1, that can be created by the flip of a spin $1/2$ neutron, are not the Goldstone modes of higher dimensions as there is no symmetry breaking. They are better thought of as composite objects of pairs of spin $1/2$, 'spinons', in that they give a response that is a continuum. Spinons can be thought of as domain walls between opposite antiferromagnetic domains that can propagate independently. As the momentum transfer from the neutron can be distributed between the two spinons, this gives rise to a continuous range of energies for given transfer rather than the single energy peak that would be seen if the triplet were an elementary excitation.

In Fig. 1(a) and (c) we sketch the regions of inelastic response for spin $1/2$ and spin 1 chains. This distinction between half-integer and integer spin chains is beautifully illustrated by neutron inelastic scattering in compounds such as $KCuF_3$ [8,9] ($s = 1/2$) and $CsNiCl_3$ [10] or NENP [2] ($s = 1$). In $KCuF_3$ the boundaries of inelastic response follow clearly the theoretical limits, as seen in Fig. 1(b), which therefore illustrates the reality of spinons. For spin one the 'Haldane gap' is clearly seen as a well defined mode for wave vectors around the antiferromagnetic vector ($q = \pi$). What remains less clear experimentally is that this mode, predicted to have zero width at zero temperature for wave-vectors above some critical value, should disappear into a continuum of states for smaller wave vector transfer. In contrast to spin $1/2$, there is yet to be a clear experimental demonstration of the continuum [10].

An alternative way to understand the alternation of the physics for half-integer and integer spin is, instead of varying the value of the spin at each site of a chain, to take 'ladders' of spin $1/2$ chains: $n = 2, 3, 4$ parallel chains with interactions along the infinite chain direction that may or may not be comparable to the transverse coupling between the n chains (see Fig. 2(a) and (b)). In increasing n to large values, we can study the crossover from a small number of chains to the infinite two-dimensional plane. The connection between spin s in a chain and the properties of $n = 2s$ parallel chains of spin $1/2$ was made in the early days of bosonization [11]. For appropriate couplings n even and odd will correspond to integer and half-integer spin respectively. Experimentally there are very nice examples of chains

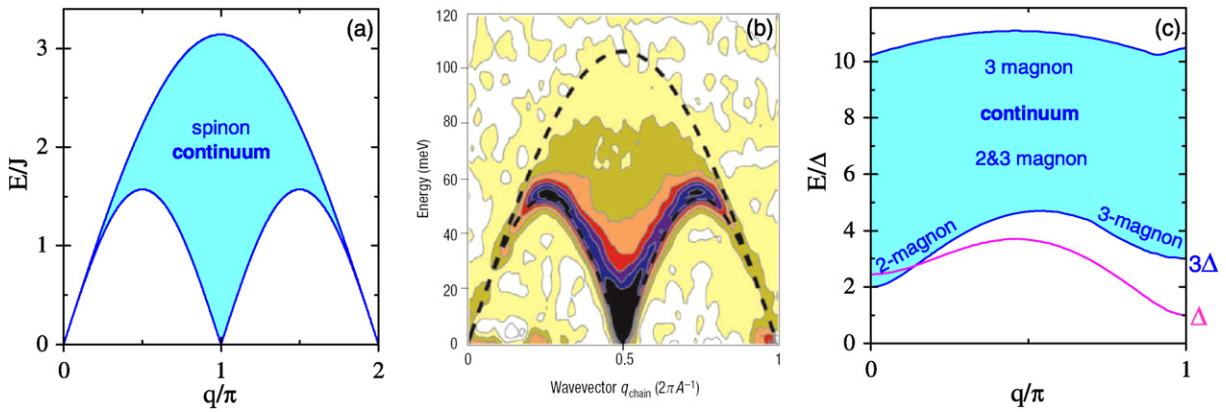

Fig. 1. Excitations in spin 1/2 and spin 1 chains: (a) theoretical prediction and (b) neutron inelastic scattering measurements in $KCuF_3$ (taken from Ref. [9]) for spin 1/2, (c) theoretical prediction for spin 1. The pink line in figures (c) corresponds to elementary excitations with width in energy that is resolution limited (outside the continuum), while the blue lines in figure (a) and (c) are the limits of the continuum of none-zero scattering intensity. Fig. (b) shows experimentally the divergence of the intensity at the lower limit of the continuum, as expected theoretically.

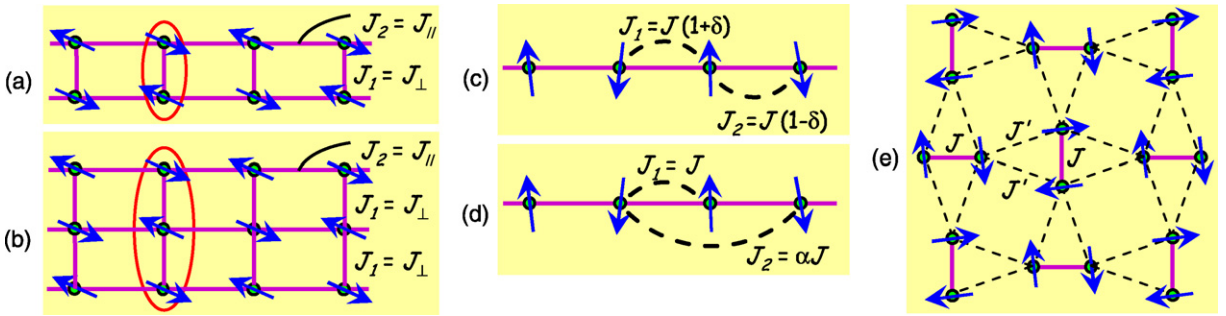

Fig. 2. (Color online) Schematic view of spin ladder with (a) $n = 2$ and (b) $n = 3$, (c) alternating chain, with δ defining the relative strength of the alternation, (d) frustrated chain, with α the relative strength of second to first nearest neighbor interaction, defining the frustration, and (e) the Shastry–Sutherland lattice: The exact ground state up to a critical value of $J' \sim 0.65$ is simply a product of singlets on each of the bonds of coupling J. The couplings shown in the different figures define the $J_{i,j}$ interactions of Eq. (1).

of copper ions $SrCu_2O_3$ ($n = 2$), $Sr_2Cu_3O_5$ ($n = 3$) [12], and $La_2Cu_2O_5$ ($n = 4$) [13]. As mentioned above, one of the motivations of studying low dimensional magnetism is to understand magnetism in two-dimensional copper oxide planes. If there is indeed a convergence between the properties of ladders and infinite planar systems it is obvious to look for ways to dope, or otherwise introduce carriers into such systems. The discovery of superconductivity in Ca-doped $Sr_{14}Cu_{24}O_{41}$ under pressure [14] was therefore exciting. An even more direct connection to the physics of copper oxide planes is via the models of 'stripes' [15] used by some groups to describe the magnetism of doped planes. The effective magnetic model is of magnetic ladders coupled weakly in the transverse direction.

For simple Heisenberg models, the distinction between integer and half-integer spins is clearly seen in the existence, or not, of a gap to excitations for chains with nearest neighbor interactions. For more general interactions, when the unit cell of the magnetic ions is larger or when there are frustrating interactions, the situation is more complex and the nature of the quantum ground state and excitations depends on the exact coupling. For example, in spin 1/2 chains, either a structural dimerization of the lattice (e.g. $CuGeO_3$ [16]) or an alternation of the intra-chain interaction (e.g. $Cu(NO_3)_2{\cdot}2.5H_2O$ [17], see Fig. 2(c)) or for sufficiently large frustrating second nearest neighbor interaction ($\alpha > 0.2411$ [18], see Fig. 2(d)), spontaneous formation of singlet that lowers the symmetry leads to a singlet ground state with a gap. The spinons that interact weakly in the uniform case acquire a stronger interaction and can form bound states giving triplet states well defined in energy as well as continuum at higher energies. If, on the other hand, a spin one chain has alternation (see Fig. 2(c)), the gap may vanish at a critical value ($\delta_c = 0.25$) representing a quantum critical point between the Haldane phase and a phase of coupled $s = 1$ dimers [19]. Model compounds illustrating these points have been studied in detail (e.g. NENP with $\delta = 0$ [2], NTEAP with $\delta = \delta_c$ [20], NTENP

with $\delta = 0.4$ [21]). Dimerization in practice involves coupling to the lattice (e.g. $CuGeO_3$) or to the charge (e.g. NaV_2O_5 as we shall see later). Finally, we mention studies of more complicated 1D systems: the tetrahedron chain $Cu_2Te_2O_5Br_2$ [22], the diamond chain azurite $Cu_3(CO_3)_2(OH)_2$ [23], ..., characterized by strong frustration between the various intra-chain interactions.

1.3. 2D and 3D spin gapped systems

In two spatial dimensions long range magnetic order will occur, at least at zero temperature, even for Heisenberg spins, and non magnetic phases can be found, for example for the square lattice only when there is strong frustration [24]. Even the triangular lattice with nearest neighbor interactions is probably ordered but the consensus is that the Kagomé lattice is so dilute that quantum fluctuations are sufficient to destroy magnetic order [25]. This has lead to interesting neutron scattering results interpreted as evidence of spinons in 2D, although this cannot be considered conclusive. An interesting planar lattice based on interacting dimers where there is no doubt as to the existence of a gapped phase was proposed by Shastry and Sutherland [26], who showed that for a particular pattern of dimers, coupled with intra-dimer J and inter-dimer J' couplings, as shown in Fig. 2(e), the quantum state, that is simply a product of singlet wave functions on each dimer, is the exact ground state for a finite range of $\frac{J'}{J}$. Some years later a very good realization of this lattice model was discovered [27]: $SrCu(BO_3)_2$ with planes of dimers having precisely the geometry considered by Shastry and Sutherland. The ratio of inter to intra-dimer interactions $\frac{J'}{J}$ is, at 0.62 [27], sufficiently large that it could not be considered in the perturbative regime, but is, nevertheless, within the dimer phase for pure Heisenberg interactions. In fact it is just below the estimated value of the quantum critical point (with ratio about 0.65) [28] where there is a predicted transition to what is probably some form of quadrumized state. Neutron scattering results were essential to show rather a novel aspect of the spin dynamics: Because of frustration between the dimers, magnon excitations propagate very weakly via Heisenberg interactions, and the splitting and dispersion of the low lying excitations are dominated by the relatively weak Dzyaloshinskii–Moriya interactions (terms $\vec{M}_{i,j}$ in Eq. (1) with the i, j neighbors corresponding to J' in Fig. 2(e)) as they are unfrustrated [29]. This compound continues to attract much attention because of novel aspects of multi-magnon states and the occurrence of magnetization plateaus in high magnetic field with magnetic order deduced from high field NMR [30]. The day when neutron scattering is possible at 30 T, this compound will no doubt be one of the first studied!

In three dimensions the natural generalizations of highly frustrated triangular-based geometries are the pyrochlores, structures with corner-sharing tetrahedra. Examples of these are $CsNiCrF_6$ [31] and $Re_2Ti_2O_7$ with Re a rare earth ion [32]. While Heisenberg exchange does not lead to long range order, the actual properties of the low energy physics are rather complex and depend on weaker interactions: dipole–dipole, Dzyaloshinskii–Moriya, single-ion anisotropies, ... It is possible to find quantum gapped systems in three dimensions in a more elementary way, starting from a local dimer configuration. A family of compounds to which we shall return later is $Cs_3Cr_2X_9$, in which the Cr 3/2 spins are in tightly bound dimers. Provided the inter-dimer interaction is sufficiently weak ($X = Cl, Br$), a state with the same symmetry as the dimer product state remains the ground state [33,34] and for stronger interactions with respect to the intra-dimer coupling ($X = I$), a magnetic state appears [35]. Of course unlike the Shastry Sutherland lattice, the ground state is never *precisely* a product of singlet wave functions on the dimers: There are always quantum fluctuations. In this particular family of compounds it is the strength of the local dimer coupling that gives a singlet ground state. In fact there is frustration in the couplings between dimers: this produces interesting incommensurabilities in the dispersion of magnons and the magnetic states induced by an applied field. As more general examples of singlet states in 3D, one can imagine weakly coupled clusters of total spin zero: molecular nano-magnets. While three-dimensional crystallographically, from a magnetic point of view they can equally be considered as quasi-0D. Take for example that of keplerates such as $\{Mo_{72}Fe_{30}\}$ where 30 $s = 5/2$ spins interact at the vertices of an icosidodecahedron [36]. They can be considered as 30 spins on the surface of a finite sphere. As the molecules are well isolated, these spins, which on the surface of an infinite sphere might order, have a singlet ground state separated by near lying states of $S = 1$, $S = 2$, ... This tower of states is indicative of long range magnetic order in the thermodynamic limit of an infinitely large sphere [37]. Thus we have an example of magnetic systems with singlet ground states having low-lying excited triplet states rather different from magnetic excitons.

This review will not mention organically based spin-gap systems (for a review, see Ref. [38]) simply for the reason that while advantageous for some techniques, most of them are as yet not available in sufficiently large single crystals for neutron inelastic scattering. Furthermore magnetic moments are often spread over several atoms of a molecule,

giving small cross-sections. It is to be hoped that this situation will change, no doubt first for organic materials including transition metal moments (e.g. λ-$(BETS)_2FeCl_4$ [39]), with increasing intensities of sources and future developments of powder techniques.

1.4. Real systems

While the examples mentioned have provoked the search for model systems showing behavior specific to classes of special interest, e.g. a particular spatial dimension, isotropy etc., real crystals have their own properties: For example a crystalline '1D' system is in fact a crystal with interactions much stronger in a particular lattice direction than in others. In practice, the interactions between chains or planes can be sufficiently strong to induce long range magnetic order. This is an interesting question in itself. The general approach is to treat one dimensional correlations exactly and the weak coupling in mean field theory. This is not exact but can give good predictions for phase diagrams. Experimentally, looking at a phase diagram as a function of varying field H and temperature T can give detailed information of dimensional crossover. Measurements of dispersion relations in zero field by neutron scattering provide a direct test of the low dimensionality. For example in $CuGeO_3$, which is often treated as a highly one dimensional dimerized system with an interesting competition between spin-Peierls and magnetic frustration, neutron scattering measurements of the dispersion revealed substantial dispersion perpendicular to the chains [40]. While we may be most interested in systems with weak anisotropy where gaps arise more from fluctuations than intrinsic anisotropies, in real life, anisotropies always occur from spin orbit interactions, even in orbital singlet states. Macroscopically this gives rise to Dzyaloshinskii–Moriya terms in the exchange, single-ion anisotropy, and anisotropies in the g-tensor. Only neutron scattering provides direct measures of the effects of such anisotropies throughout the Brillouin zone. Of course complementary measurements with electromagnetic probes are essential: while restricted to momentum transfer essentially $q \approx 0$, they are normally much more precise in energy. Good examples of the complementarity of optical and neutron measurements are in the studies of the field-dependent gaps in Cu-benzoate [41] and in $SrCu_2(BO_3)_2$ [42].

1.5. Field-induced magnetism

The combination of neutron scattering studies and application of external magnetic fields has always been important in magnetism. It is relatively easy to combine the techniques and the field is obviously a relevant parameter to any magnetic state. For relatively low fields, the Zeeman splitting seen by neutrons confirms the magnetic nature of multiplet excitations and gives direct evidence of anisotropies. A very nice example is that of $SrCu_2(BO_3)_2$ where not only the splitting but also the ratio of intensities of the split lines gave direct evidence of the Dzyaloshinskii–Moriya anisotropies [29]. In this, and in other systems, comparison of neutron studies and the more precise information limited to the zero wave vector of ESR was vital. Similarly NMR gives detailed information on local correlations and relaxation seen at different nuclear sites.

Apart from such studies, where variation of the magnetic field essentially provides a tool for refining our understanding of a phase at low fields, there are now examples where the field allows passage from one phase to another, entirely different, via, at zero temperature, some sort of quantum critical point. The best examples of this are probably now in the transition from a low field singlet phase to a higher field phase with spontaneous magnetic order induced transverse to the applied field. This is illustrated in Fig. 3(b), where the shaded area indicates the range of energies of magnons at different wavevectors q with dispersion (shown in Fig. 3(a)), as a function of the field. The lowest component $|1, -1\rangle(q)$ of the magnon at each vector q decreases linearly by Zeeman splitting, and when the first magnon of $q = Q_0$ vanishes in energy, at H_{c1}, there is a transition to a state with Field Induced (transverse) Magnetic Order (FIMO). While this is generally true for systems with singlet ground state, for the case of strongly bound dimers we can picture the ground state of the FIMO in local terms as being a product over the dimers of coherent superpositions of the singlet and lowest triplet states defined on each dimer. The coherent superposition of the two states generates non-zero expectation values for transverse components of spin. The phases of superposition will vary in space, giving spatial variation in the transverse components, and in the simplest approximation this variation would have the same wave-vector as the soft magnon $|1, -1\rangle(Q_0)$. Because of interactions between magnons the propagation vector of the induced structure may differ from Q_0. This induced state persists up to a saturation field H_{c2} whose distance from H_{c1} is roughly the width of the dispersive triplet band. At finite temperatures $T_C(H)$ there is a phase transition associated with the appearance of the symmetry-breaking transverse components and T_C vanishes approaching the two critical

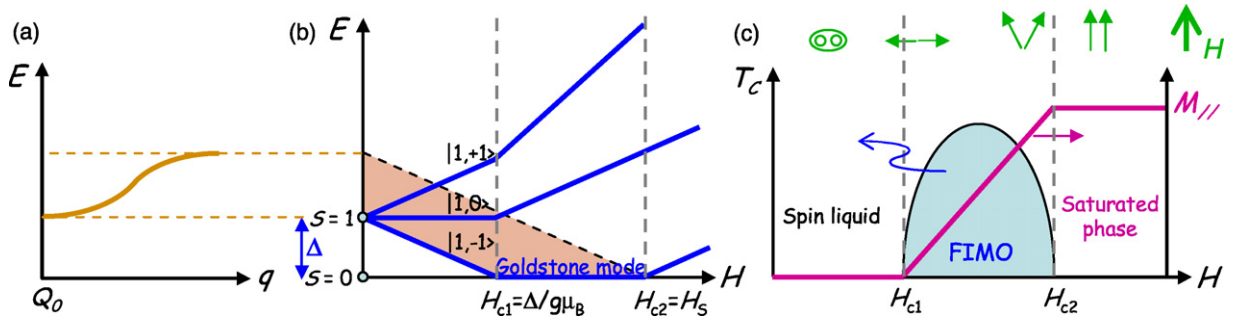

Fig. 3. (Color online) Field effects on an isotropic gapped quantum magnetic system. (a) Schematic picture of spin wave dispersion of the triplet state at zero field. (b) Field dependence of the energy gaps: Zeeman splitting up to H_{c1}, followed by a Bose–Einstein condensation up to H_{c2}, where saturation is reached; the width of the condensed phase is determined by the dispersion in zero field, as indicated schematically by the dashed area. (c) Field dependence of the critical temperature (left axis) and that of the parallel magnetization (right axis). The spin liquid (gapped) system enters below $T_C(H)$ a Field-Induced Magnetic Ordering at H_{c1} up to H_{c2}, in which a transverse ordering develops while a parallel magnetization monotonically increases up to saturation, yielding the canted spin configuration sketched above.

fields H_{c1} and H_{c2} where these components go to zero (Fig. 3(c)). The transverse component of magnetization follows qualitatively the curve drawn for T_C and the longitudinal (paramagnetic) component $M_{\parallel}(H)$ increases monotonically from H_{c1} to saturation reached at H_{c2}. Thus the FIMO state is a form of canted antiferromagnet similar to a classical antiferromagnet above the spin-flop field.

A first description of the transition to the field-induced state is as a Bose–Einstein condensation of the magnon that softens [43]. The analogy with Bose–Einstein condensation of, say, photons or helium atoms, is complicated by the different form of interactions between bosons and the presence of a crystal lattice. The magnons are pseudo-bosons rather than real bosons: i.e. their number is not necessarily conserved in interactions. Nevertheless the phenomenon in magnetic systems provides the opportunity for a detailed study of correlations and dimensional dependencies. It is particularly interesting to look at the transverse components since their phase is analogous to the phase of the condensate of superfluid Helium-4. The parallel magnetization as a function of the applied field corresponds to the helium density as a function of chemical potential. If there is substantial anisotropy in the plane perpendicular to the applied magnetic field, the analogy with superfluidity (where there is *exact* symmetry with respect to different phases) is no longer perfect. Therefore it is best to choose the most symmetric crystal direction to apply the magnetic field. Even a few years ago a full neutron study was difficult because of limitations in the magnitudes of the fields available in different configurations (horizontal versus vertical field).

The first really comprehensive study with static and dynamic correlations perpendicular to the important field directions will be fully described in Section 3, with the choice of material $s = 3/2$ $Cs_3Cr_2X_9$, dictated by the relatively low critical field for $X =$ Br (2 T). Another material which has received much attention is $TlCuCl_3$ [44]. This is somewhat simpler than the material we will consider in detail in that the spin 1/2 should be less anisotropic, but nonetheless many of the same questions are relevant: Is the Goldstone mode that we would expect from the broken continuous symmetry of the ordered phase really gapless? In $TlCuCl_3$ neutron scattering [45] can be directly compared to ESR [46] as it happens that the soft mode is at $q = 0$. As we mentioned, it is only by choosing special materials that we can attain the first magnetic fields where the magnetization becomes non-zero. It is also interesting to look for magnetization plateaus at higher field, at either fractional (e.g. Kagomé) or integer (e.g. azurite) multiples of a single saturated moment of the magnetic species per unit cell. Finally, in some materials it may be possible to apply a magnetic field sufficiently strong that the spins are totally aligned. This is extremely useful as the absence of zero point fluctuations around the fully saturated state means that measuring the dispersion of excitations determines the microscopic couplings of the Hamiltonian essentially without any approximation. A good example of this is in the $s = 1/2$ alternating chain compound $Cu(NO_3)_2{\cdot}2.5H_2O$ where the couplings determined unambiguously at high field can be used to test our understanding of the strongly correlated zero field phase [47].

1.6. What is the special contribution of neutrons to the above?

It is well known that neutron scattering is a powerful technique particularly for magnetism but we shall nonetheless review the fundamental reasons for this. Historically, even though many steady-state sources are the same as at the time

of the review of 1976 [1], advances in instrumentation and sample environment have improved the quality of the data enormously. Nowadays, magnetic fields up to 15 T (17 T without dilution) and 4 T can be applied, perpendicular and parallel, respectively, to a horizontal scattering plane, even at dilution temperatures, for both single-crystal diffraction and triple-axis spectroscopy. These limitations are due to the necessity of using split coils to allow access to the neutron beam. Pressure cells allow one to measure typically up to 30 kbar for reasonably large samples (30 mm^3) and up to 500 kbar for very small samples (0.01 mm^3). In addition, new spallation sources extend the energy range to allow, for example, the spectacular images of Fig. 1(b). The neutron is electrically neutral so it can penetrate deeply in matter and interact with the nuclei of the atoms, by the nuclear interaction. Second, the neutron carries a spin 1/2, and thus a small magnetic moment $\mu_n = 1.913\ \mu_{BN}$ (nuclear Bohr magneton): It can thus also strongly interact with the moments of electronic origin (unpaired electrons), which are about a thousand times larger than μ_n.

The neutrons produced in a nuclear reactor or in a spallation source have a typical wavelength of 0.4 to 10 Å, that is of the same order of magnitude as the typical inter-atomic distances in condensed matter. Therefore, neutrons are perfectly suited for elastic scattering (i.e. diffraction): They allow us to determine crystallographic and magnetic structures. Contrary to X-rays, for which the magnetic diffracted intensity is about 10^6 times smaller than the nuclear one, the nuclear and magnetic scattered amplitudes are comparable for neutrons, so that in practice, magnetic structures are almost exclusively determined by neutron diffraction. In addition to the structural Bragg peaks located at positions $\mathbf{H} = (h, k, l)$ of the reciprocal space ($h,\ k,\ l$ integers), a magnetic structure will give rise to additional peaks at scattering vectors $\mathbf{Q} = \mathbf{H} + \mathbf{k}$, where $\mathbf{k}$ is the propagation vector of the magnetic structure. The propagation vector describes how the magnetic structure propagates in the lattice from cell to cell (e.g. $\mathbf{k} = \mathbf{0}$ for a ferromagnet, $\mathbf{k} = (1/2, 1/2, 0)$ for a simple antiferromagnet with a doubling of the cell along the a and b directions, and no doubling along the c direction). The integrated intensities of the magnetic Bragg peaks give the information about the spin arrangement within the unit cell: spin direction relative to the crystallographic axes and between the various magnetic atoms of the cell, and value of the magnetic moment. Fig. 4(a) gives a scheme of the typical diffractometer used for magnetic structure determination or phase diagram study on a single crystal mounted in a magnetic field. The determination of a magnetic structure will be illustrated by the example presented in Section 3.

Neutrons also have a typical energy of 0.8 to 600 meV, that is in the energy-range of most excitations in condensed matter (phonons, magnons, ...). Thus, when the neutron is inelastically scattered, its energy change corresponds to a large fraction of its incident energy. Inelastic scattering can therefore bring precise information on excitation energies and thus on the inter-atomic forces, in the case of nuclear scattering (e.g. phonons), and on the magnetic interactions, in the case of magnetic scattering (e.g. magnons). Neutrons and X-rays have the huge advantage of allowing one to select a specific momentum transfer $\hbar\mathbf{Q}$ together with a specific energy transfer $\hbar\omega$, contrary to other techniques, such as ESR or Raman that can only measure at $Q = 0$, or NMR that as a local probe, integrates over all Q's and investigates much smaller energies. This feature is particularly important in some of the transitions to be considered here: for example spin-Peierls transitions in the simplest models occur at band edge phonons. If X-rays and neutrons are both adapted to study phonons, X-rays have not been used to study magnons due to a too weak intensity (excitations have a much weaker intensity than Bragg peaks). Thus, neutron inelastic scattering is, in practice, a unique tool to study the dispersion of magnetic excitations. In scattering, the total spin (neutron plus sample) is conserved, so that the neutrons can exchange either zero or one unit of spin. From measuring the dynamical structure factors $S(\mathbf{Q}, \omega)$, one can obtain the spin dispersion (from the position in $\mathbf{Q}$ and ω of the excitation), as well as the intensity of energy-integrated structure factor $S(\mathbf{Q})$. From these two quantities, as will be illustrated by the two selected examples presented in Sections 2 and 3, one can determine the exchange interactions (not only Heisenberg interaction but also anisotropic ones such as e.g. Dzyaloshinskii–Moriya or single-ion anisotropy), demonstrate frustration or some extended form factors (in the case of a delocalized electron). Also, neutron inelastic scattering is an ideal technique to study a continuum of magnetic excitations, which are of special importance in low-dimensional magnetism where the elementary excitation can be an excitation of spin half (a spinon). The neutron must then create spinon pairs to exchange a unit of spin. Fig. 4(b) gives a scheme of the typical spectrometer used for such inelastic measurements on a single crystal.

Finally, let us mention that the use of polarized neutrons is even more powerful, though it will not be illustrated here. In diffraction, it is widely used to determine spin density maps, taking the advantage that the magnetic (M) signal is enhanced by the nuclear (N) one, due to interference NM terms. Moreover, by analyzing the final polarization of neutrons, one can solve completely certain complex magnetic structures for which unpolarized neutron diffraction

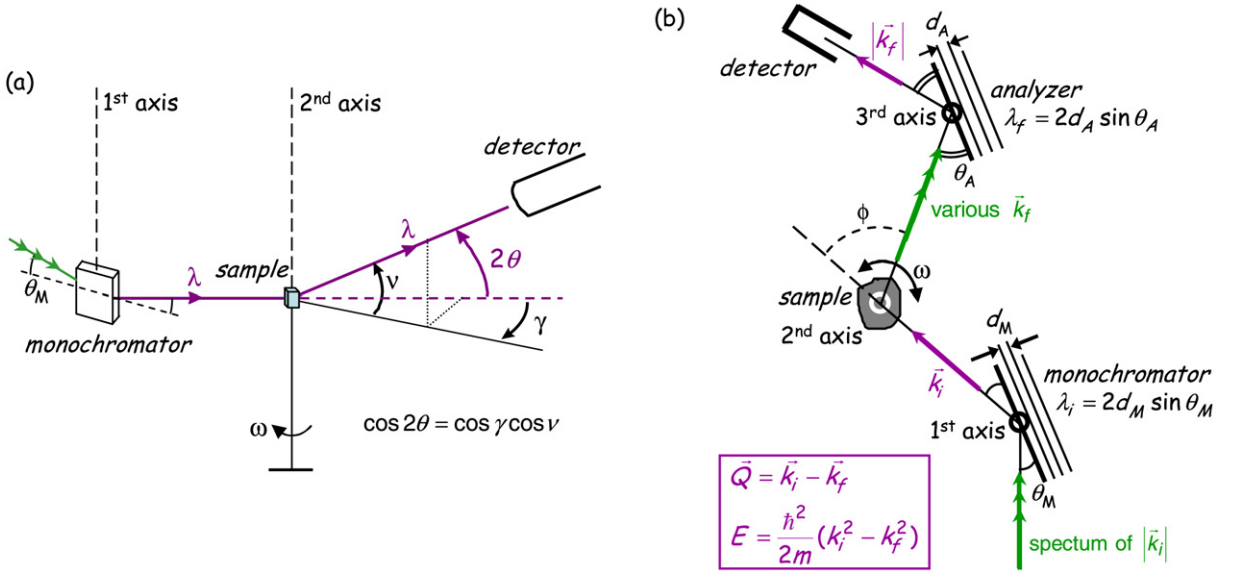

Fig. 4. (Color online) (a) Schematic drawing of a lifting-counter two-axis diffractometer, used for neutron diffraction on single-crystals. Once the incident wavelength has been chosen (by rotating the monochromator around the first vertical axis to an angle θ_M), one can select various Bragg peaks by rotating the sample around the second vertical axis (angle ω) and turning the detector in the horizontal plane (angle γ) and outside of this plane (angle ν). A rocking curve (i.e. an intensity versus ω measurement) is performed for each peak, and then integrated over ω to obtain the intensity. Note that the diffracted neutrons of different wavelengths have negligible intensity, as compared to (elastically) diffracted neutrons, so that they just give a background contribution. (b) Schematic drawing of a triple-axes spectrometer (top view), used for neutron inelastic scattering on single-crystals. The scattering plane is strictly horizontal, and a third vertical axis is now added (analyzer) in order to select a specific scattered wave vector, with different modulus from the incident one for inelastic scattering. By changing the two angles of each of the three axes (monochromator, sample, and analyzer), one can select a specific scattering vector $\mathbf{Q}$ and a specific energy transfer $\hbar\omega$. In practice, one makes energy-constant Q-scans and/or Q-constant energy scans: the peaks in the neutron counts $S(Q,\omega)$ correspond to the excitations.

leaves ambiguities. Fully polarized neutron inelastic scattering allows to separate magnetic from nuclear contributions (e.g. magnons from phonons), and in the future, to measure mixed nuclear-magnetic correlation functions [48].

2. First selected example: the spin-ladder compound NaV_2O_5

The low dimensional inorganic compound NaV_2O_5 undergoes a phase transition at $T_c = 34$ K [49] associated with both a lattice distortion [50] and the opening of an energy gap to the lowest triplet spin excitations [51]. This was originally thought to be the second inorganic example, after $CuGeO_3$, of a spin-Peierls transition. It has turned out that neither compound is so simple: In $CuGeO_3$ magnetic frustration is very important and in NaV_2O_5 charge order (CO) dominates. Formally the vanadium orbitals have charge $+4.5\,e$ so that naïveley, i.e. in thinking of an effective single band model with one d orbital per V atom, it may seem obvious that charge order is likely. We shall see that the picture that emerges, from neutron and other results, is considerably more subtle. Returning to a possible analogy with $CuGeO_3$, however, we *could* imagine a possible reduction to a half-filled model, as follows: In the high temperature structure, the vanadium atoms form a ladder structure with V–O–V 'rungs' in the a direction, coupled in the b direction [52]. A possibility, likely in the absence of strong correlation, would be that the final half electron per V atom occupied a bonding V–O–V orbital. Projecting out the anti-bonding combination on each rung, this gives an effective model in a single band which is now half-filled, i.e. each ladder would be equivalent to a spin $1/2$ Heisenberg chain (see Fig. 5(a)). Then comparing bonding V–O–V orbitals to half-filled copper orbitals in $CuGeO_3$, we might expect a similar form of spin-Peierls transition, via coupling to the phonons, at lower temperature.

This picture is *not* consistent with experiments, however: NMR measurements indicated two inequivalent vanadium sites below T_c, compared to one site above [53,54]. This suggests a quite different mechanism, likely if we consider only V orbitals but assume that the dominant terms are Coulomb interactions within each d orbital, between d orbitals across a rung, and between d orbitals on adjacent rungs (i.e. along the ladder legs). For a physically reasonable model with stronger Coulomb repulsions within the ladder rungs and from rung to rung along the b direction rather than

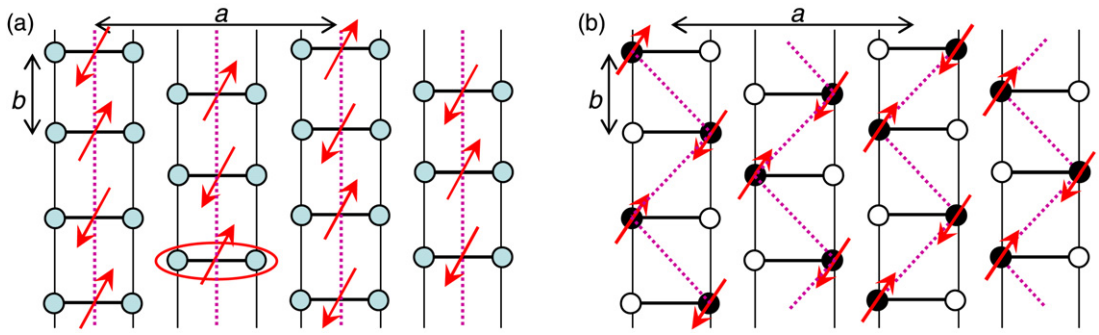

Fig. 5. (Color online) Sketch of the NaV_2O_5 ladders, where only the vanadium atoms are represented, (a) in the high temperature phase, with (blue) circles representing $V^{+4.5}$, and (b) in a low temperature phase of zig-zag order with complete charge disproportionation, with the full and empty circles representing, respectively, V^{+4} and V^{+5}. These two states can be viewed as in-line or zig-zag spin 1/2 Heisenberg chains, respectively, as indicated by the dotted (purple) lines.

diagonally, this can favor a zig-zag pattern of charges 5+ ($s = 0$), 4+ ($s = 1/2$) [55], as shown in Fig. 5(b). This explains very plausibly the inequivalence of the sites. Again there can be a reduction to a spin-Peierls mechanism via elimination of the 5+ orbitals and a lattice distortion reflecting the zig-zag order. Thus we have two different, relatively simple, possible mechanisms for spin-gap formation at low temperature and it would seem straightforward to determine which is the accurate picture. An accurate account has emerged, through a combination of neutron, X-ray and NMR results which, at a quantitative level, is far from either of the two simple pictures of Fig. 5(a) and (b). All of these studies revealed that the charge order was not total, but the problem arose that *neither* taken literally is consistent *quantitatively* with apparently contradictory values of the zig-zag order parameter (quite large from neutron inelastic scattering [56] as we shall see hereafter, very small from NMR [54] and X-rays [57]). The final picture [58] is a synthesis in that it combines physical elements of both images: The zig-zag nature of the wave function and V–O–V hybridization are both central.

As NMR is a local measurement, scattering experiments, by neutrons and by X-rays, were necessary to determine the actual distribution of charges in the gapped phase and to produce a microscopic theory of the spin gap. Only through a combination of these techniques has a coherent picture of the spin gap emerged. X-ray diffraction measurements [59] suggested a lattice structure below T_c described by the $Fmm2$ space group with a $(2a \times 2b \times 4c)$ unit cell, consisting of a succession of distorted and non-distorted ladders of vanadium ions, which would give rise to three different V valences (4+ and 5+ in the distorted ladders, 4.5+ in the non-distorted ones). Doubt was cast, however, by other experimental results, in particular the observation by NMR of only two inequivalent V sites [53,54] but as many as 8 Na sites [60]. This is in contradiction both with the existence of three different V sites and the space group $Fmm2$, respectively. Later on, both X-ray diffraction [61] and anomalous X-ray scattering [62] studies showed that all ladders are modulated and that different stacking sequences along the c direction coexist in the structure. As a result, the structure proposed by Lüdecke et al. [59] is an average of this stacking structure. It is now well accepted that the correct structure at low-T is monoclinic rather than orthorhombic (space group $A112$) [61] with a two times smaller unit cell as initially proposed ($\mathbf{a}' = \mathbf{a} - \mathbf{b}$, $\mathbf{b}' = \mathbf{2b}$, $\mathbf{c}' = \mathbf{4c}$) and all the ladders distorted (see Fig. 6(a)). Let us now review the neutron inelastic scattering results of the spin excitations in the low-T phase [56] that were central to showing the apparent contradictions in the values of charge order and also their resolution. The interpretation given here is more complete than in the original publication, thanks to the newer structure of Sawa et al. [61] to be compared to that known at the time [59], to later work on anomalous X-ray scattering and to quantum chemical calculations.

The basis of the interpretation of the neutron inelastic scattering results to deduce charge order was the comparison of the intensities of the spin wave scattering as a function of scattering vector Q along a, that is transverse to the ladder direction. In fact the spin wave excitations are strongly dispersive along the ladder direction (b-axis), and the low frequency components around the zone centre and zone boundary for the b direction (Q_b integer and half-integer, resp.) were used to exploit the better resolution at these frequencies. This allowed us to deduce a 'form factor' within each rung, for the electrons participating in the spin excitation. At the time we interpreted the results by means of a simplified form of charge distribution involving only the V atoms (with their magnetic d orbital only). Comparing calculated to measured intensities allowed determination of the effective charge transfer from left to right or right to

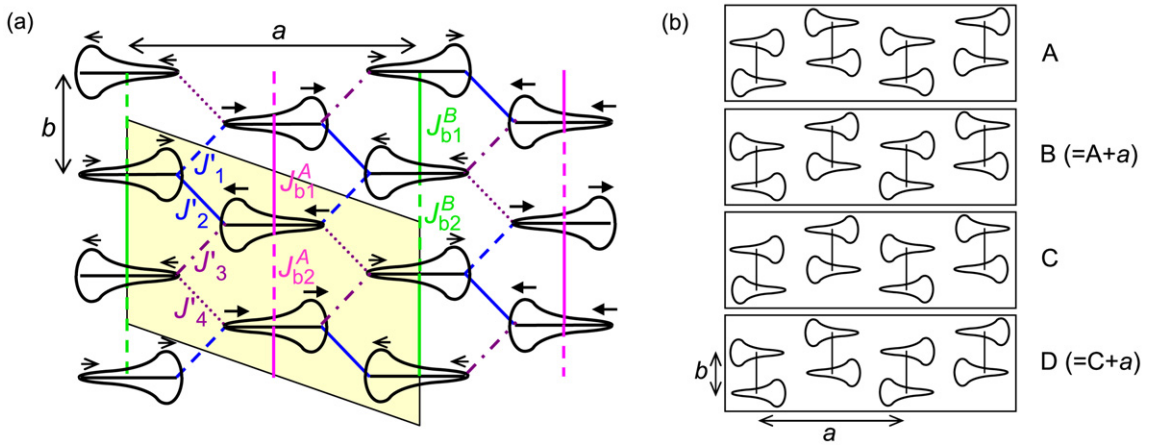

Fig. 6. (Color online) (a) Sketch of one possible charge order (labeled C or D in figure (b)) in the (a, b) plane. The large and small lobes represent large and small average charges: this partial charge order is intermediate between those of Fig. 5(a) and (b), so that the (red) ellipse from Fig. 5(a) is now replaced by an asymmetric object. In addition, there are lattice displacements of V atoms, different in the two ladders, indicated by the arrows. The low-T cell ($\mathbf{a}' = \mathbf{a} - \mathbf{b}$, $\mathbf{b}' = \mathbf{2b}$) is shown in the (yellow) parallelogram. This charge order leads to the two distinct observed spin gaps and the elementary translation $\mathbf{a} \pm \mathbf{b}$ of this CO agrees with the observed periodicity of spin excitations. (b) The four possible different charge-ordered planes, consistent with the neutron inelastic scattering results: B and D are obtained from A and C, respectively, by applying a translation $\mathbf{a}$.

left of each V–O–V rung and the arrangements of these CO patterns from rung to rung along and transverse to the ladders. We will make this more explicit a little later, once the main neutron inelastic scattering results are presented.

2.1. *Neutron inelastic scattering results*

The inelastic scattering measurements were performed at Institut Laue Langevin (ILL) on the thermal neutron triple-axes spectrometer IN22 [63] (see Fig. 4(b) for a schematic drawing of the instrument), using a large NaV_2O_5 single crystal, cooled down well below T_c, at $T = 5$ K. A wide set of energy scans (as shown in Fig. 7(a)) were performed at constant scattering vectors $\mathbf{Q} = (Q_a, Q_b, 0)$ for many Q_a components ranging between 0 and 5 r.l.u. (relative lattice units, i.e. $5a^*$) and for Q_b chosen either at the zone center ($Q_b^{ZC} = 1$) or boundary ($Q_b^{AF} = 0.5, 1.5$), for the reasons mentioned above. Note that the components Q_a and Q_b are expressed in the reciprocal lattice of the orthorhombic high temperature ($a \times b \times c$) unit cell. Two distinct excitations were clearly observed on most of the energy-scans, with an unsymmetrical line shape characteristic of gapped excitations undergoing a rapid energy dispersion (along b). Using an appropriate dynamical response function, all these scans could be well fitted (see solid lines) allowing to extract, for both excitations (labelled $+$ and $-$), the position in energy $E_{\pm}^{AF,ZC}$ and the integrated intensity of the fitted function over a wide energy-range, that is, the individual structure factors $S_{b\pm}^{AF,ZC}(Q)$. This analysis yielded the dispersion curves presented in Fig. 7(b) along the a direction and the Q_a dependence of the individual and total structure factors $S_b^{AF}(Q_a) = S_{b+}^{AF}(Q_a) + S_{b-}^{AF}(Q_a)$ and $S_b^{ZC}(Q_a) = S_{b+}^{ZC}(Q_a) + S_{b-}^{ZC}(Q_a)$ plotted in Fig. 7(c). We shall now explain in detail what crucial information could be learned from these two results.

As can be seen in Fig. 7(b), two distinct excitation branches are clearly observed, well separated in energy over all the Q_a range, with a maximum of the lower branch $E_g^- \simeq 9.1$ meV and a minimum of the upper branch $E_g^+ \simeq 10.1$ meV. Note that in earlier neutron inelastic scattering observations [51], which could not separate these two extrema due to a poorer energy resolution, the two branches were thought to cross each other, yielding a periodicity two times larger for the dispersion and a single energy gap. As will be shown here, the existence of two, and not one, distinct energy gaps, and the knowledge of the correct periodicity for the dispersion played a crucial role in the understanding of the phase transition and in the determination of possible charge orders.

First, from the periodicity found in our dispersion curves, we could propose the zig-zag charge order sketched in Fig. 6(a) (labeled C or D in Fig. 6(b)), as well as the symmetry related (by changing a into $-a$) A or B patterns. The Q_a dependence of the structure factors (see below) allowed us to rule out an in-line CO. Second, the observation of two distinct energy branches proves the existence of two inequivalent alternating chains. Charge order alone would give equivalent alternating chains; thus the splitting comes from lattice distortions. This is true both for the newer

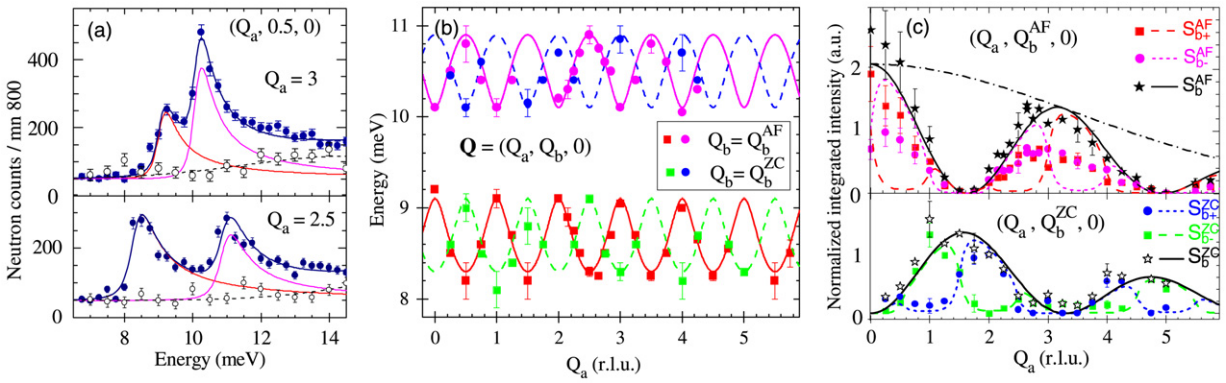

Fig. 7. (Color online) (a) Examples of constant-Q energy scans (closed circles) and background (open circles) determined from Q_b-scans at same Q_a and various energies. The solid lines are fit to the data as described in text. (b) Spin dispersion of the two excitation branches along the a direction at zone center Q_b^{ZC} and boundary Q_b^{AF}. The curves are theoretical predictions [56] fitted to the data (solid symbols). (c) Q_a-dependence of the structure factors $S_{b\pm}^{AF}$ and $S_{b\pm}^{ZC}$ for the upper (+) and lower (−) branches at Q_b^{AF} and Q_b^{ZC} and of their sums S_b^{AF} and S_b^{ZC} (closed and open symbols). The data are corrected from the V^{4+} atomic form factor and normalized at $Q_b = 0.5$ (dot-dashed line). The other curves are theoretical predictions compared to the data (see text).

structure [61] and the older [59]. Taking into account the CO sketched in Fig. 6(a) and the newer structure, this yields four different transverse couplings J_i' ($i = 1, 2, 3, 4$) between the two types of ladders, as shown in the same figure. Their sequence in the b direction differs from one ladder to the other, thus implying two different sets of couplings along the ladder legs and, therefore, two inequivalent alternating ladders. The transverse dispersion of the two branches could then be derived, involving the two energies E_g^+ and E_g^- and the alternation in the inter-ladder diagonal bonds $\delta J = J_1' - J_2' + J_3' - J_4'$. The spin dispersions could be very well fitted (see solid and dashed lines in Fig. 7(b)), yielding $\delta J = 1.2$ meV (to be compared to the average coupling along the ladder legs, $J_b \simeq 60$ meV, determined from the stiff spin dispersion along b [56]). E_g^+ and E_g^- can be interpreted as the gaps for the two *isolated* ladders. From estimates of the gap produced by the measured charge order, as discussed below, the conclusion is that in NaV_2O_5, the gaps are *primarily* due to the CO while the lattice distortion plays a secondary role, explaining why two distinct branches are observed experimentally, and their separation.

We now come to the analysis of the structure factors. In our simplified analysis involving only the vanadium magnetic $3d$ orbitals, a charge disproportionation $\Delta_c = 0.6$ (i.e. $V^{4.2+}$, $V^{4.8+}$) could be deduced on each rung based on the expression [56]: $S_{Q_b}(Q_a) = \cos^2(\pi Q_a \rho)\tilde{S}(Q_a, Q_b) + \Delta_c^2 \sin^2(\pi Q_a \rho)\tilde{S}(Q_a + \frac{1}{2}, Q_b + \frac{1}{2})$ for the total structure factor, where $\rho = l/a \approx 0.304$ (l, rung length and a, lattice parameter) and $\tilde{S}(Q_a, Q_b)$ would be the structure factor for spins localized at the center of each rung [64]. As seen in Fig. 7(c), the agreement is good both for $S_b^{AF}(Q_a)$ and $S_b^{ZC}(Q_a)$. Note that from the ratios of intensities for different values of momentum, one can extract the charge transfer $\delta = \Delta_c/2$ independently of the form of $\tilde{S}$. In addition, this served to rule out other forms of charge order that had been proposed. For the individual intensities, we needed an explicit form for $\tilde{S}$, e.g. from the strongly dimerized limit. This allowed structure factors to be calculated within each branch, as shown by the dashed lines in Fig. 7(c). The agreement with the data was rather good at the zone center. In particular, the extinction phenomenon observed for each branch was well reproduced. However, there was one difficulty at the AF position which was noted at the time but not resolved: While the sum $S_b^{AF}(Q_a)$ was well described, there was a discrepancy between calculated and measured *individual* structure factors $S_{b+}^{AF}(Q_a)$ and $S_{b-}^{AF}(Q_a)$. This was an interesting point which was resolved later thanks to the deduction of the *three dimensional* structure.

In our analysis we assumed one of four different symmetry related forms of charge order (shown in Fig. 6(b)), but the more recent anomalous X-ray diffraction study of Ref. [62] has shown that the ladder planes are in fact stacked along the c direction with the two coexisting sequences: either BDAC and DBCA or BBAA and DDCC. Therefore, one has to average the individual structure factors coming from each type of plane. For symmetry reasons, one easily finds that it is equivalent to replacing $S_{b\pm}^{AF,ZC}(Q_a)$ by $\frac{1}{2}[S_{b\pm}^{AF,ZC}(Q_a) + S_{b\pm}^{AF,ZC}(-Q_a)]$. This now gives the correct result at the zone boundary (with $S_{b\pm}^{AF}(Q_a)$ odd functions of Q_a and $S_{b\pm}^{AF}(-Q_a) = S_{b\mp}^{AF}(Q_a)$), while it yields the same result at the zone center (since $S_{b\pm}^{ZC}(Q_a)$ are even functions of Q_a). Thus the X-ray structure in 3 dimensions

resolved a slightly puzzling aspect of the self consistency of some of the results raised in the previous neutron study. The estimate $\Delta_c \approx 0.6$ was based on the *total* intensities and was thus unaffected. The charge transfer was also shown to explain the magnitude of the spin gap [56]. While this worked reasonably well, it was phenomenological in the sense that no microscopic argument for the magnitude of the charge order was provided.

The really puzzling aspect of the results at that time was that the charge transfer was found to be quite large from neutron inelastic scattering, while in NMR [54] and later resonant X-ray studies [57], it had been deduced to be very small ($\delta = 0.04\,e$ from Ref. [57]). The key idea to make a fully coherent description of all techniques came from quantum chemical calculations of clusters of atoms and their orbitals [65]. What emerged was that fluctuations in the occupations of bridging oxygen p orbitals should be significant [66] and this had been totally neglected in the analysis of the neutron results. Thus while the form factors correctly described interference coming from amplitudes on the different V orbitals contributing to the magnetic scattering, they did not 'see' contributions to the charge from essentially non-magnetic orbitals. Thus what was measured was really the charge disproportionation projected onto the magnetic moments only. The NMR and resonant X-rays, on the other hand, probed all the charge fluctuations, allowing the magnitude of the charge order to appear smaller. The fuller wave function, with both V and oxygen bands can give a microscopic justification for the very small charge order, the essential effect at the transition being a reorganisation of the 3d orbitals population within the V atoms [58].

2.2. Conclusions for first considered example

The investigation of NaV_2O_5 by neutrons, NMR and X-rays has been rewarding in that it gives an essentially quantitative description of an interesting strongly correlated system. There is a wider significance in that apparent contradictions on a measured quantity 'the charge disproportionation' from various techniques gave clues to the nature of the wave function, and in particular the role of oxygen orbitals, often considered as essentially passive transmitters of magnetic exchange. A rather similar mechanism of weak charge disproportionation has recently been deduced in the context of manganites [67].

3. Second selected example: the spin 3/2 dimer compound $Cs_3Cr_2X_9$ (X = Br, Cl)

This system corresponds to the case of gapped quantum system in a field described in Fig. 3, except that due to the 3/2 spin value of Cr, two other FIMO's can be expected at higher field, when the gaps from higher excited states $S = 2$ and $S = 3$ close. $Cs_3Cr_2X_9$ crystallizes in an hexagonal structure with two dimers of Cr^{3+} ions per unit cell, oriented along the **c**-axis and arranged in planes perpendicular to **c** [68]. The intra-dimer J and inter-dimer J_p and J_c (in-plane and out-of-plane) magnetic couplings (shown in Fig. 9(a)) were determined from the dispersion of the triplet measured by neutron inelastic scattering in zero field [33,34]. The larger ratio of the intra- to the inter-dimer couplings ($J/(6J_p + 3J_c) \simeq 6.1$ for Cl, $\simeq 2.3$ for Br) gives a higher energy gap in zero field for Cl than for Br, and thus a higher critical field. Inagaki et al. [69] have measured the magnetization curves in both compounds at $T = 0.5$ K, for the field applied along the **c**-axis (see Fig. 8(a)). The first critical field is indeed much higher for Cl: $H^i_{c1} \simeq 12.3$ T, to be compared to $H_{c1} \simeq 2$ T for Br. Moreover, the Cl compound has two magnetization plateaus before saturation, and is thus characterized by three distinct FIMO's (*simple*-FIMO's) between H^i_α and H^f_α ($\alpha = 1, 2, 3$). On the contrary for X = Br, no magnetization plateau is seen: there is a unique FIMO (*extended*-FIMO, i.e. the three simple-FIMO's overlap), a direct consequence of a smaller ratio of intra- to inter-dimer couplings. The decreasing widths of the plateaus in the $M(H)$ curve for Cl could be well explained by introducing some biquadratic exchange in the Hamiltonian [69,70]. The magnetization for $H \perp c$, measured in the Br compound (see green solid triangles in Fig. 8(c)), reveals sizable anisotropy ($H_{c1} \simeq 1.4$ T, smaller than H_{c1} for $H \parallel c$).

$Cs_3Cr_2X_9$ differs from other dimer systems that are currently studied by neutron scattering (e.g. PHCC [71], $TlCuCl_3$ [45]) in two important ways: each Cr^{3+} ion of the dimer has spin 3/2 rather than 1/2 for Cu-based systems and, because of the hexagonal arrangement of the dimers, the inter-dimer couplings are frustrated. The higher spin means that the anisotropy, always present in magnetic systems, is likely to be greater and thus its effect on Bose–Einstein condensation can be seen more easily. The frustration means that the bosons that condense have incommensurate wave vectors that lie on a degenerate line in the (a^*, b^*) plane of reciprocal space (plotted in red on the contour plot of excitations from Fig. 8(b)). This last effect raises interesting theoretical questions that are not yet

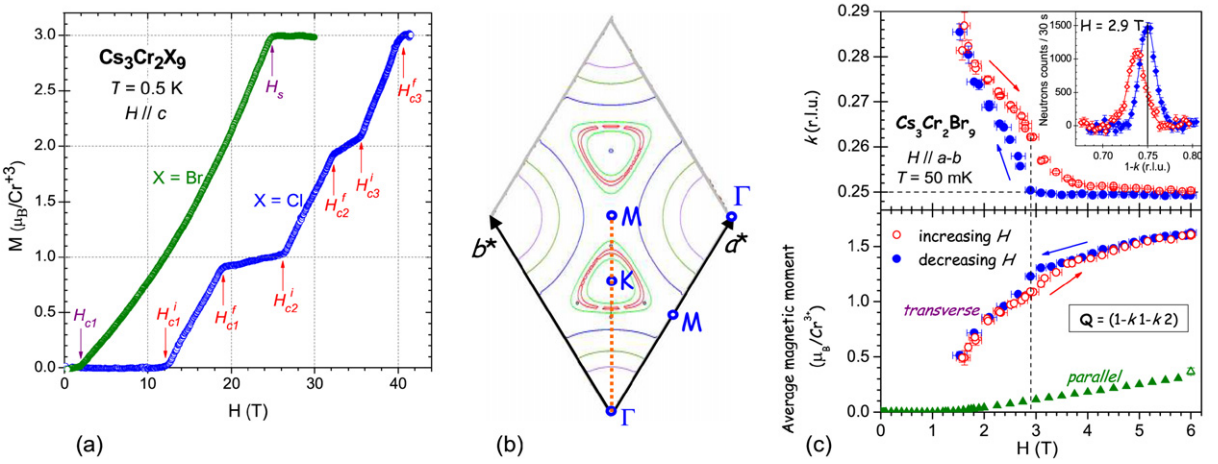

Fig. 8. (Color online) (a) Magnetization curves measured at $T = 0.5$ K for $H \parallel c$ in $Cs_3Cr_2X_9$ (X = Cl, Br). In the case of Cl, two distinct plateaus are clearly seen, evidencing the presence of 3 *simple*-FIMO's, while for X = Br, no plateau is seen, due to an overlap of the 3 FIMO's resulting in an *extended*-FIMO. (b) Contour plot of excitations in the (a^*, b^*) plane: the Γ, K, M points are local maxima, the red line is the line of continuous degenerate minima. The dashed (orange) line indicates the 110 direction. (c) Field-dependence of the propagation wave-vector component k (top panel) and that of the parallel and transverse magnetizations (lower panel) in $Cs_3Cr_2Br_9$ for $\mathbf{H} \parallel \mathbf{a} - \mathbf{b}$. The inset shows Q-scans performed across the $(3/4, 3/4, 0)$ magnetic peak at $H = 2.9$ T for increasing and decreasing field along the $\mathbf{a} + \mathbf{b}$ direction: Hysteresis effects and incommensurabilities are clearly seen.

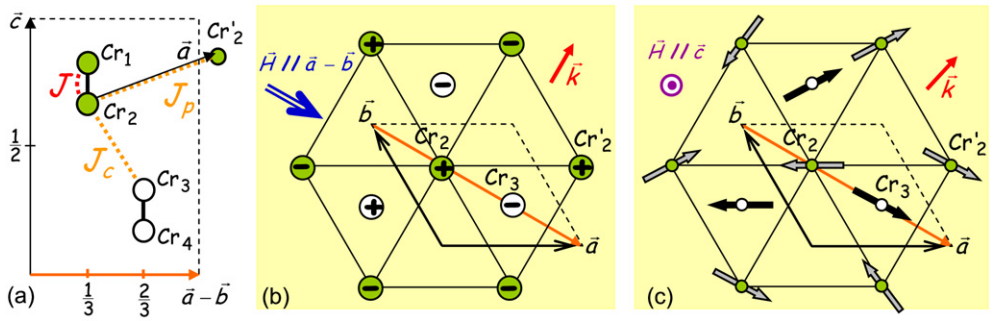

Fig. 9. (Color online) (a) Arrangement of the Cr^{3+} dimers in the hexagonal unit cell of $Cs_3Cr_2X_9$ (X = Br, Cl) and magnetic couplings: a Cr atom of a dimer (J coupling) is coupled to 6 neighbors from the same plane (through J_p) and 3 neighbors from the neighboring plane (through J_c). Transverse spin ordering shown for Cr_2 and Cr_3 for (b) $H \parallel \mathbf{a} - \mathbf{b}$ in the Br compound at 6 T and in the Cl one at 15 T, (c) $H \parallel \mathbf{c}$ in the Br compound at 6 T. Within a dimer, the spins are antiparallel for both field orientations.

fully resolved (see the discussion in Ref. [70]). For example, how is the magnetic order above H_{c1} related to the **Q** vectors of the softest magnons before condensation? Clearly, only neutron scattering can study this question in detail.

These were the motivations for looking at the compounds $Cs_3Cr_2X_9$ (X = Cl, Br). The opportunity to do so was especially interesting, as only recently has there been the possibility of doing neutron scattering experiments up to 15 T and down to 50 mK. In particular, this allows the study of the Cl compound, with a large first critical field of 12.2 T and a maximum in $T_{c1}(H)$ at 800 mK and 16 T. In order to see in detail the effect of the anisotropy, two different field orientations have been exploited in $Cs_3Cr_2Br_9$ (the compound with the lowest critical field) [72]: $H \parallel \mathbf{a} - \mathbf{b}$ and $H \parallel \mathbf{c}$, i.e. perpendicular and parallel to, as will be shown here, the easy-axis **c**. In order to clarify the impact of the nature of the FIMO (*extended vs simple*), the two compounds, X = Br [73] and X = Cl [74], were studied, with the same field orientation, $H \parallel \mathbf{a} - \mathbf{b}$. The neutron diffraction experiments were performed at ILL on the lifting-counter two-axes diffractometer D23 and the neutron inelastic scattering ones on the cold neutron triple-axes spectrometers IN12 and IN14 [63] (see Fig. 4(a) and (b) for a schematic drawing of these instruments). Various state of the art cryomagnets were used: 6 T vertical and 4 T horizontal for Br, 15 T vertical for Cl, equipped with a dilution insert.

3.1. Magnetic structure

Neutron diffraction allowed us to determine the transverse spin ordering in the FIMO. The transverse magnetic structure was found to have a commensurate propagation vector $\mathbf{k} = (1/4, 1/4, 0)$ for $H \parallel \mathbf{a} - \mathbf{b}$, at 6 T for Br and 15 T for Cl, and an incommensurate one, $\mathbf{k} = (0.426(2), 0.148(2), 0)$ for $H \parallel \mathbf{c}$, at 6 T for Br. Their two equivalent propagation vectors, by symmetry, were also observed. A wide set of magnetic peaks were collected in the three domains to allow the magnetic refinement. For both field orientations and both compounds, the three magnetic domains were found to be roughly equally populated and the spin arrangement antiparallel within a dimer. For $H \parallel \mathbf{a} - \mathbf{b}$, the collinear $++--$ magnetic structure depicted in Fig. 9(b) was obtained, assuming a constant moment amplitude. The AF moments of 1.58(1) μ_B (resp. 0.79(1) μ_B) per Cr^{3+} ion at 6 T for $X = Br$ (resp. at 15 T for $X = Cl$) point along the c-axis, thus identified as being the easy-axis. Applying the field along the c-axis makes this anisotropy ineffective in breaking axial symmetry, and indeed a very different magnetic structure was found for $X = Br$, still at 6 T: the cycloid depicted in Fig. 9(c), with constant AF moments rotating in the $(a,\ b)$ plane. A moment amplitude of 1.75(1) μ_B per Cr^{3+} ion was deduced, with a phase difference of $0.422(2) \times 2\pi$ between Cr_2 and Cr_3 from the same unit cell, close to the $0.426(2) \times 2\pi$ angle between two adjacent Cr_2 ions when moving along the a direction.

For both field orientations (H perpendicular and parallel to the easy-axis c), the AF magnetic structure corresponds indeed to a transverse ordering. Although these two orderings differ in important ways—the first is commensurate and collinear, differing in both respects from the second—, they also show some strong similarities: In both cases, one pair of spins out of three, intra- and inter-plane, is aligned in parallel, even though J_p and J_c are antiferromagnetic, evidencing some frustration, while the sum of the two others is antiparallel. Let us emphasize that the determination of these transverse orderings, which is possible by neutron diffraction, is of crucial importance to give a complete description of the frustration and anisotropy, and thus to explain the spin dynamics in the FIMO. The parallel magnetization could also be determined from the ferromagnetic contribution appearing on top of a weak nuclear Bragg peak (see the open green triangle in Fig. 8(c), obtained from the $(1, 1, 4)$ reflection in the Br compound at 6 T for $H \parallel \mathbf{a} - \mathbf{b}$): It allows to check agreement with magnetization measurements.

The field dependence of the propagation wave-vector and that of the AF transverse magnetic moment $M_\perp$ were studied in both compounds for $\mathbf{H} \parallel \mathbf{a} - \mathbf{b}$, by following a strong magnetic peak. Practically, Q-scans were performed in the (110) direction across the strongest magnetic peak $(1 - k,\ 1 - k,\ 2)$ with $k \sim 0.25$, for increasing and decreasing magnetic field H. Then, k and $M_\perp$ could be accurately obtained from fitting each scan by a Gaussian function: The position gives the wave-vector component k and the square-root of the intensity gives $M_\perp$. As can be seen in figure 8(c) (solid and open circles), coming from 6 T, the transverse commensurate $++--$ ordering of $Cs_3Cr_2Br_9$ remains locked down to $H \sim 3$ T ($k = 0.25$) and then becomes incommensurate (k varies progressively up to 0.29 for $H = 1.5$ T, that is slightly above H_{c1}), suggesting pinning [75]. For increasing H, however, the commensurate $++--$ structure is reached only at $H \sim 5$ T, which, interestingly, indicates a large hysteresis. These two effects can be clearly seen on the scans shown in the inset of Fig. 8(c), where the magnetic peak is recorded for the same field value, $H = 2.9$ T, while H is increased or decreased. On the contrary, no hysteresis and no incommensurabilities were observed in $Cs_3Cr_2Cl_9$ from 15 T down to 12.2 T [72]: The propagation vector remains $(1/4, 1/4, 0)$. Also, the field dependence of the transverse magnetic intensity close to H^i_{c1} was found to be much sharper as in the case of bromide.

The observation for $X = Br$ and the absence for $X = Cl$ of incommensurabilities remains unclear. Nevertheless, it should be related to the position $(Q_0, Q_0, 2)$ of the energy gap along the 110 direction (see Fig. 8(b), where the dashed orange line intercepts the contour in red), as compared to that of the propagation vector in high field. Indeed, the first minimum of the dispersion curve occurs at $Q_0 \simeq 0.27 \neq k$ for $X = Br$ [73], but at $Q_0 = 0.25 = k$ for $X = Cl$ [74]. Note that this hysteretic effect for Br was only visible on the transverse moment, so that only neutron diffraction could reveal this interesting feature of the FIMO.

3.2. Spin dynamics

Neutron inelastic scattering is also an essential tool for: (i) studying the spin-wave dispersion of the triplet excitation in zero field, in order to quantify the exchange couplings, isotropic and anisotropic, and (ii) following the energy gaps (minima of the dispersion curves) as a function of field, in order to study the Zeeman splitting and especially the FIMO, with the essential question: does the gap close or not?

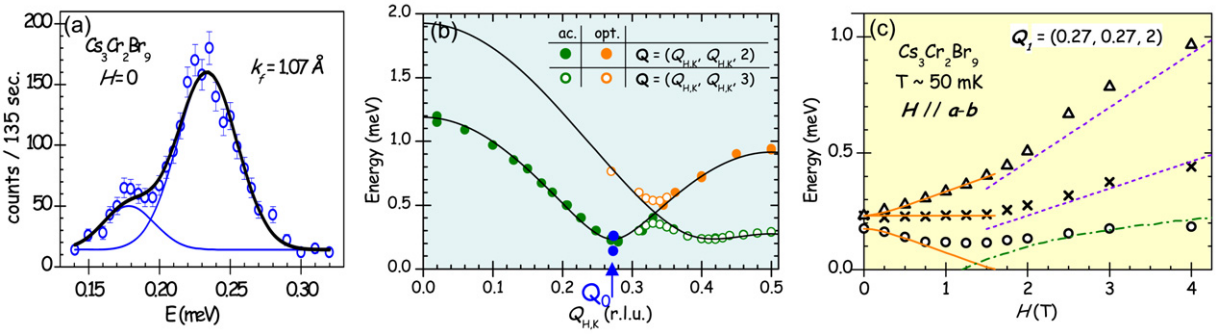

Fig. 10. (Color online) Neutron inelastic scattering measurements in $Cs_3Cr_2Br_9$. (a) Q-constant energy scan at $H = 0$ measured at $\mathbf{Q} = (Q_0, Q_0, 2)$ with an improved resolution ($Q_0 = 0.27$), evidencing the splitting of the $S = 1$ state. (b) Spin-wave dispersion along the $\mathbf{a} + \mathbf{b}$ direction showing the positions of the energy gaps and evidencing an anticrossing between the optic (opt.) and acoustic (ac.) branches. (c) Field dependence of the three energy gaps for $H \parallel \mathbf{a} - \mathbf{b}$. The various lines are described in the text.

Fig. 10(b) displays the dispersion curves measured in zero field for the Br compound along the $\mathbf{a}^* + \mathbf{b}^*$ direction (solid and open circles) and their fit by the same expression as in Ref. [34] (solid lines) which allows to extract the J, J_c and J_p couplings. The presence of two Cr^{3+} dimers per unit cell gives rise to two distinct branches while the two minima (energy gaps) mentioned before can be clearly seen, around $(0.27, 0.27, 2)$ and $(0.41, 0.41, 2)$ along the (110) direction. Looking in more detail at the positions of the energy gap ($Q_{H,K} = 0.27$) and that where the two branches join ($Q_{H,K} = 0.33$), the two following new results (not seen previously [34]) were obtained thanks to the improved resolution now available: (i) the two excitation branches show an anticrossing, which remains to be explained, (ii) more important, a splitting of the $S = 1$ triplet, $\Delta E = 0.056$ meV, is clearly observed on the energy scan from Fig. 10(a) performed at $(0.27, 0.27, 2)$ with a higher resolution (using a smaller final wave vector k_f). This splitting is accounted for by a single-ion anisotropy term $D(s_i^c)^2$ at each Cr^{3+} site with $D \simeq -0.01$ meV $\sim -J/100$, which confirms the easy-axis character of the c-axis assumed from the previous diffraction results in the FIMO. In the Cl compound, the energy gap at $(0.25, 0.25, 2)$ is at much larger energy, $\simeq 1.4$ meV, so that unfortunately, neither splitting of the triplet nor anticrossing of the two branches could be tested for comparison. These results emphasize the power of neutron scattering, that can give a direct evidence and estimation of the anisotropy, but also the limitations due to the rather poor energy-resolution that can be achieved on a triple-axes spectrometer ($\delta E/E \sim 10^{-1}$ for a reasonable flux, that is with no collimation but only with optimized k_f).

Let us now focus on the field effects on the spin dynamics. For both compounds, and for both field orientations in the case of Br, we found from dispersion curves measurements performed at a few field values up to the maximum accessible one, that the Q_0 positions of the energy gaps are field-independent, even though the propagation wave vector of the magnetic structure is changing for Br. So we present the field dependence study of the energy gaps for the three branches of the $S = 1$ state, obtained from energy-scans at $(Q_0, Q_0, 2)$. Particular attention was paid to correct the data by subtraction of the background (the tail of the incoherent scattering) to the low energy part of the scans. This was feasible only down to 0.05 meV, putting a limit of 0.07 meV for the lowest observable gap. Fig. 10(c) presents the energy gaps *vs* H results obtained in $Cs_3Cr_2Br_9$ for $\mathbf{H} \parallel \mathbf{a} - \mathbf{b}$. The Zeeman splitting observed below H_{c1} is very well fitted for the three branches using the value of D derived in zero-field (see solid orange lines) and yields an expected critical field of 1.5 T for $H \parallel \mathbf{a} - \mathbf{b}$, in good agreement with the diffraction data. For $H > H_{c1}$, three distinct energy branches are still observed. The upper two agree roughly with Zeeman behaviors (dashed purple lines), while the lowest remains gapped: It is non-zero even at H_{c1} ($\epsilon_g \sim 0.11$ meV) and increases up to 0.19 meV at 4 T. The gap in the FIMO phase can be accounted for, at least qualitatively, by the presence of single-ion anisotropy along c, i.e. in the plane perpendicular to the applied field [73] (see dot-dashed green line, for which the calculated $\epsilon_g(H)$ curve was multiplied by a factor of 5). The 5 times too large value of the gap in the FIMO was ascribed to the *extended* nature of the FIMO, implying a mixing of higher order states ($S = 2$ and $S = 3$), which were not taken into account in the theoretical description proposed in Ref. [73].

To test these two hypotheses, that is the role of the anisotropy and that of the *extended*-FIMO, the same study was performed in the Br compound for the other field orientation and in the Cl compound for the same field orientation. For $H \parallel \mathbf{c}$, the single-ion anisotropy does not break axial symmetry around the field direction and, in consequence,

should not create a gap. Indeed, the remaining gap observed in $Cs_3Cr_2Br_9$ at H_{c1} is very small or may even vanish ($\epsilon_g < 0.05$ meV), but surprisingly, it increases above H_{c1} to reach the *same* value of 0.19 meV at 4 T [72], although one might now expect a gapless Goldstone mode throughout the magnetic phase. To explain this, one could perhaps invoke some small anisotropy in the (a, b) plane and, again, the effect of the *extended*-FIMO, that amplifies the observed gap. In the Cl compound, the simple description considering only the lowest branch of the $S = 1$ state and the $S = 0$ state should now better describe the results, since the three FIMO's are distinct. Indeed, the remaining gap $\epsilon_g < 0.05$ meV observed at $H = 12$ T $\simeq H^i_{c1}$ is much smaller than for Br ($\epsilon_g \sim 0.11$ meV at 2 T) and reopens only up to 0.13 meV at 15 T, to be compared to 0.21 meV for Br at 5 T, that is 3 T above the first critical field. We now lack the value of the single-ion anisotropy in the Cl compound, in order to estimate the expected gap and thus check whether the nature of the FIMO can explain alone the discrepancy for Br. Last, the ideal test would be of course to measure the spin dynamics in the FIMO of the Cl compound for $\mathbf{H} \parallel \mathbf{c}$, where we have the best chance to observe a Bose–Einstein condensation. But this is unfortunately impossible for technical reasons: The magnetic field has to be applied in the horizontal plane of the triple-axes spectrometer, but the maximum available field for a split horizontal magnet is only 4 T (due to enormous stray fields), which puts a limit to what can be done actually. But we keep the hope such an experiment to be possible in the future, with all the developments taking place to always access more extreme conditions.

3.3. Conclusions for second example

This example has illustrated the completeness of the study that can be performed with neutron scattering. This complementary study of the magnetic ordering and the spin dynamics, as a function of the applied field, with the possibility to choose the field direction, to test anisotropy effects, and to vary the X element (Cl or Br), to look in detail at the nature of the FIMO, yields a better understanding of this interesting system. Our comparison shows explicitly the relation of the energy gap to the transition to the FIMO: For Cl, with commensurate Q_0, there is neither hysteresis nor incommensurabilities, contrary to Br. In addition, the gap really closes at H^i_{c1}, but reopens substantially immediately after, a behavior which remains to be explained quantitatively. The existence of a continuous degenerate line of soft magnons and the anisotropies force us to generalize the Bose–Einstein condensation description for real magnetic systems.

4. General conclusions

While two examples out of the many possibilities currently studied cannot be said to be representative, we can attempt nonetheless to draw some more general conclusions. One is that while sometimes the increasing power of alternative techniques might seem to threaten the preeminence of neutron scattering in magnetism, this is unlikely to be the case. Advances in resonant X-ray scattering, in particular, allow increasingly valuable comparisons for some elements and allow more precise conclusions to be drawn from neutron scattering studies. While the intensity of the new generation of pulsed sources of neutrons will give new information, especially at higher energies, even 'incremental' improvements in instrumentation can be of equal importance. In the first example taken, crucial information of analysis was in the *intensity* of inelastic scattering: The extraction of such intensities from the background has necessitated continuous instrument development. The further elimination of background by pulsed sources could be as important as increases in peak intensity. In that example the intensities allowed for information on the (magnetic) electron wave function. Another example in the literature where the variation of intensity was crucial, is in spin ladder systems where it has been argued that it allowed separation of two-magnon from one-magnon scattering [76]. The second example shows the importance of developing superior sample environment and crossed techniques; in particular the availability of higher magnetic fields has opened up new domains of physics for exploration. We can hope for static fields considerably larger (30 T) than those available and there is even the demonstration that pulsed fields (at 40 T) can be used in conjunction with coincidence techniques for magnetic diffraction [77]. An aspect that we have hardly touched on is the use of the analysis of the full polarization for both elastic and inelastic scattering. Here the instruments already exist (for example at the ILL, several instruments can be equipped with the 'Cryopad' device) and are in use in zero external magnetic field. They have been used in diffraction to resolve ambiguities in complex magnetic structures. For Polarised Neutron Inelastic Scattering, the full exploitation remains to be made: In principle there should be significant new information on cross-correlations between nuclear and magnetic scattering [48]. The

feeling is that there are significant new discoveries to be made, but the appropriate systems are yet to be found. For a recent review of experimental results, see Ref. [78].

Predicting the future in terms of subjects and concepts is probably even more hazardous than anticipating instrumental development. Extrapolating from current trends, it seems likely that there will continue to be many new magnetic materials to be characterized with neutron scattering as well as more detailed studies of materials already identified. This is true within the class of materials we have focussed on: systems without long range magnetic order at zero field, where many aspects, such as doping effects and coupling between magnetism and transport, modifications under field and pressure, remain to be elucidated. For comparison with detailed theories, while quasi-one dimensional materials can be analysed with the help of very detailed quantitative calculations, the same is not true in two and three dimensions. It remains to be seen whether concepts, such as topological and fractional excitations can be made sufficiently quantitative that detailed comparison is possible with experimental systems. If we enlarge the discussion to more general magnetic systems, particularly interesting for material properties will be those combining magnetic properties with others: ferroelectricity, semiconducting transport properties and so on. There are materials which are well studied by other techniques, but where, up to now, single crystals sufficiently large to allow detailed study by neutrons have not been grown. As crystals become larger and fluxes increase these may have renewed importance: Organic conductors with and without transition metals come to mind [38]. Artificially structured and inhomogeneous materials are of enormous current interest and again the problems of techniques suited most to single homogeneous crystals must be circumvented. An example where this is already happening is in dilute magnetic semiconductors where most samples are inhomogeneous films; recent studies using grazing incident polarised neutron reflectrometry have yielded profiles of magnetic and structural scattering transverse to the surface of the film [79]. This is also an example where history dependent properties of non-equilibrium samples can be revealed. One can imagine other likely applications: Neutron scattering for samples subject to applied laser excitation may well lead to exciting new physics. A recent example used an applied laser with neutron Laue diffraction to study photo-induced phase transitions in a molecular magnet [80].

References

[1] M. Steiner, J. Villain, C.G. Windsor, Adv. Phys. 25 (1976) 87.
[2] J.P. Renard, M. Verdaguer, L.P. Regnault, W.A.C. Erkelens, J. Rossat-Mignot, W.G. Stirling, Europhys. Lett. 3 (1987) 945.
[3] D. Visser, A.R. Monteith, S.G. Carling, T. Zeiske, J. Appl. Phys. 81 (1997) 4399 and references therein.
[4] See e.g. A.M. Tsvelick, Quantum Field Theories in Condensed Matter Physics, Cambridge University Press, Cambridge, England, 1995.
[5] H. Bethe, Z. Phys. 71 (1931) 205;
R. Baxter, Exactly Solved Models in Statistical Mechanics, Academic Press, London, 1982.
[6] F.D.M. Haldane, Phys. Rev. Lett. 50 (1983) 1153.
[7] J. Des Cloizeaux, J.J. Pearson, Phys. Rev. 128 (1962) 2121.
[8] S.E. Nagler, D.A. Tennant, R.A. Cowley, T.G. Perring, S.K. Satija, Phys. Rev. B 44 (1991) 12361 and references therein.
[9] B. Lake, D.A. Tennant, C.D. Frost, S.E. Nagler, Nature Mater. 4 (2005) 329.
[10] I.A. Zaliznyak, S.-H. Lee, S.V. Petrov, Phys. Rev. Lett. 87 (2001) 017202 and references therein;
I.A. Zaliznyak, J. Appl. Phys. 91 (2002) 8390.
[11] H.J. Schulz, Phys. Rev. B 34 (1986) 6372.
[12] M. Azuma, Z. Hiroi, M. Takano, K. Ishida, Y. Kitaoka, Phys. Rev. Lett. 73 (1994) 3463.
[13] K. Kudo, T. Noji, Y. Koike, T. Nishizaki, N. Kobayashi, J. Phys. Soc. Jpn. 72 (2003) 2551.
[14] M. Uehara, T. Nagata, J. Akimitsu, H. Takahashi, N. Môri, K. Kinoshita, J. Phys. Soc. Jpn. 65 (1996) 2764;
H. Mayaffre, P. Auban-Senzier, M. Nardone, D. Jérome, D. Poilblanc, C. Bourbonnais, U. Ammerahl, G. Dhalenne, A. Revcolevschi, Science 279 (1998) 345.
[15] See e.g. J.M. Tranquada, cond-mat/0512115 (unpublished);
D.X. Yao, E.W. Carlson, D.K. Campbell, Phys. Rev. B 73 (2006) 224525 and references therein.
[16] M. Hase, I. Terasaki, K. Uchinokura, Phys. Rev. Lett. 70 (1993) 3651;
J.-P. Pouget, L.-P. Regnault, M. Aïn, B. Hennion, J.-P. Renard, P. Veillet, G. Dhalenne, A. Revcolevschi, Phys. Rev. Lett. 72 (1994) 4037;
For a review, see: J.-P. Boucher, L.-P. Regnault, J. Phys. I France 6 (1996) 1939–1966.
[17] J.C. Bonner, S.A. Friedberg, H. Kobayashi, D.L. Meier, H.W. Blöte, Phys. Rev. B 27 (1993) 248 and references therein.
[18] K. Okamoto, K. Nomura, Phys. Lett. A 169 (1992) 433.
[19] S. Yamamoto, Phys. Rev. B 51 (1995) 16128.
[20] Y. Narumi, K. Kindo, M. Hagiwara, H. Nakano, A. Kawaguchi, K. Okunishi, M. Kohno, Phys. Rev. B 69 (2004) 174405.
[21] M. Hagiwara, L.P. Regnault, A. Zheludev, A. Stunault, N. Metoki, T. Suzuki, S. Suga, K. Kakurai, Y. Koike, P. Vorderwisch, J.-H. Chung, Phys. Rev. Lett. 94 (2005) 177202 and references therein.

[22] M. Johnsson, K.W. Törnroos, F. Mila, P. Millet, Chem. Mater. 12 (2000) 2853–2857;
P. Lemmens, K.-Y. Choi, E.E. Kaul, C. Geibel, K. Becker, W. Brenig, R. Valenti, C. Gros, M. Johnsson, P. Millet, F. Mila, Phys. Rev. Lett. 87 (2001) 227201.
[23] H. Kikuchi, Y. Fujii, M. Chiba, S. Mitsudo, T. Idehara, T. Tonegawa, K. Okamoto, T. Sakai, T. Kuwai, H. Ohta, Phys. Rev. Lett. 94 (2005) 227201 and references therein.
[24] H.-J. Schulz, T. Ziman, Europhys. Lett. 18 (1992) 355.
[25] G. Misguich, C. Lhuillier, in: H.T. Diep (Ed.), Frustrated Spin Systems, World Scientific, Singapore, 2004.
[26] B.S. Shastry, B. Sutherland, Physica B & C 108 (1981) 1069.
[27] H. Kageyama, K. Yoshimura, R. Stern, N.V. Mushnikov, K. Onizuka, M. Kato, K. Kosuge, C.P. Slichter, T. Goto, Y. Ueda, Phys. Rev. Lett. 82 (1999) 3168.
[28] S. Miyahara, K. Ueda, Phys. Rev. Lett. 82 (1999) 3701.
[29] O. Cépas, K. Kakurai, L.P. Regnault, T. Ziman, J.P. Boucher, N. Aso, M. Nishi, H. Kageyama, Y. Ueda, Phys. Rev. Lett. 87 (2001) 167205.
[30] K. Kodama, M. Takigawa, M. Horvatic, C. Berthier, H. Kageyama, Y. Ueda, S. Miyahara, F. Becca, F. Mila, Science 298 (2002) 395.
[31] M.P. Zinkin, M.J. Harris, T. Zeiske, Phys. Rev. B 56 (1997) 11786.
[32] T. Fennell, O.A. Petrenko, B. Fåk, J.S. Gardner, S.T. Bramwell, B. Ouladdiaf, Phys. Rev. B 72 (2005) 224411.
[33] B. Leuenberger, H.U. Güdel, J.K. Kjems, D. Petitgrand, Inorg. Chem. 24 (1985) 1035.
[34] B. Leuenberger, A. Stebler, H.U. Güdel, A. Furrer, R. Feile, J.K. Kjems, Phys. Rev. B 30 (1984) 6300.
[35] B. Leuenberger, H. Güdel, P. Fischer, Phys. Rev. B 33 (1986) 6375.
[36] A. Müller, M. Luban, C. Schröder, R. Modler, P. Kögerler, M. Axenovich, J. Schnack, P. Canfield, S. Bud'ko, N. Harrison, Chem. Phys. Chem. 2 (2001) 517.
[37] O. Cépas, T. Ziman, Progr. Theor. Phys. 159 (2005) 280.
[38] H. Seo, C. Hotta, H. Fukuyama, Chem. Rev. 104 (2004) 5005.
[39] L. Brossard, R. Clerac, C. Coulon, M. Tokumoto, T. Ziman, D. Petrov, V. Laukhin, M.J. Naughton, A. Audouard, F. Goze, A. Kobayashi, H. Kobayashi, P. Cassoux, Eur. Phys. J. B 1 (1998) 439–452.
[40] L.P. Regnault, M. Aïn, B. Hennion, G. Dhalenne, A. Revcolevschi, Phys. Rev. B 53 (1996) 5579.
[41] D.C. Dender, P.R. Hammar, D.H. Reich, C. Broholm, G. Aeppli, Phys. Rev. Lett. 79 (1997) 1750;
T. Asano, H. Nojiri, Y. Inagaki, J.P. Boucher, T. Sakon, Y. Ajiro, M. Motokawa, Phys. Rev. Lett. 84 (2000) 5880.
[42] H. Nojiri, H. Kageyama, K. Onizuka, Y. Ueda, M. Motokawa, J. Phys. Soc. Jpn. 68 (1999) 2906;
T. Rõõm, U. Nagel, E. Lippmaa, H. Kageyama, K. Onizuka, Y. Ueda, Phys. Rev. B 61 (2000) 14342.
[43] I. Affleck, Phys. Rev. B 43 (1991) 3215.
[44] A. Oosawa, M. Ishii, H. Tanaka, J. Phys.: Condens. Matter 11 (1999) 265;
H. Tanaka, A. Oosawa, T. Kato, H. Uekusa, Y. Ohashi, K. Kakurai, A. Hoser, J. Phys. Soc. Jpn. 70 (2001) 939.
[45] Ch. Rüegg, N. Cavadini, A. Furrer, H.-U. Güdel, K. Krämer, H. Mutka, A. Wildes, K. Habicht, P. Vorderwisch, Nature (London) 423 (2003) 62.
[46] V.N. Glazkov, A.I. Smirnov, H. Tanaka, A. Oosawa, Phys. Rev. B 69 (2004) 184410.
[47] B. Grenier, J.-P. Boucher, J.-Y. Henry, L.-P. Regnault, T. Ziman, J. Magn. Magn. Mater. 310 (2007) 1269–1271.
[48] S.V. Maleev, Phys. Uspekhi 45 (2002) 569.
[49] M. Isobe, Y. Ueda, J. Phys. Soc. Jpn. 65 (1996) 1178;
M. Weiden, R. Hauptmann, C. Geidel, F. Steglich, M. Fischer, P. Lemmens, G. Güntherodt, Z. Phys. B 103 (1997) 1;
Y. Fujii, H. Nakao, T. Yosihama, M. Nishi, K. Nakajima, K. Kakurai, M. Isobe, Y. Ueda, H. Sawa, J. Phys. Soc. Jpn. 66 (1997) 326.
[50] T. Chatterji, K.D. Liß, G.J. McIntyre, M. Weiden, R. Hauptmann, C. Geibel, Solid Stat. Comm. 108 (1998) 23;
A. Meetsma, J.L. de Boer, A. Damascelli, J. Jegoudez, A. Revcolevschi, T.T.M. Palstra, Acta. Cryst. C 54 (1998) 1558.
[51] T. Yosihama, M. Nishi, K. Nakajima, K. Kakurai, Y. Fujii, M. Isobe, C. Kagami, Y. Ueda, J. Phys. Soc. Jpn. 67 (1998) 744.
[52] H.G. Von Schnering, Y. Grin, M. Kaupp, M. Somer, R.K. Kremer, O. Jepsen, T. Chatterji, M. Weiden, Z. Kristallogr. 213 (1998) 246.
[53] T. Ohama, H. Yasuoka, M. Isobe, Y. Ueda, Phys. Rev. B 59 (1999) 3299.
[54] Y. Fagot-Revurat, M. Mehring, R.K. Kremer, Phys. Rev. Lett. 84 (2000) 4176.
[55] M. Mostovoy, D. Khomski, cond-mat/9806215;
H. Seo, K. Fukuyama, J. Phys. Soc. Jpn. 67 (1998) 2602.
[56] B. Grenier, O. Cépas, L.P. Regnault, J.E. Lorenzo, T. Ziman, J.P. Boucher, A. Hiess, T. Chatterji, J. Jegoudez, A. Revcolevschi, Phys. Rev. Lett. 86 (2001) 5966.
[57] Y. Joly, S. Grenier, J.E. Lorenzo, Phys. Rev. B 68 (2003) 104412.
[58] M.-B. Lepetit, et al., Preprint, 2007.
[59] J. Lüdecke, A. Jobst, S. van Smaalen, E. Morré, C. Geibel, H.-G. Krane, Phys. Rev. Lett. 82 (1999) 3633.
[60] T. Ohama, A. Goto, T. Shimizu, E. Ninomiya, H. Sawa, M. Isobe, Y. Ueda, J. Phys. Soc. Jpn. 69 (2000) 2751.
[61] H. Sawa, E. Ninomiya, T. Ohama, H. Nakao, K. Ohwada, Y. Murakami, Y. Fujii, Y. Noda, M. Isobe, Y. Ueda, J. Phys. Soc. Jpn. 71 (2002) 385.
[62] S. Grenier, A. Toader, J.E. Lorenzo, Y. Joly, B. Grenier, S. Ravy, L.P. Regnault, H. Renevier, J.Y. Henry, J. Jegoudez, A. Revcolevschi, Phys. Rev. B 65 (2002) 180101.
[63] A detailed presentation of the various neutron spectrometers can be found at: http://www.ill.fr/YellowBookCDrom/index.htm.
[64] O. Cépas, Ph.D. Thesis, University Joseph Fourier, Grenoble, France, 2000.
[65] N. Suaud, M.B. Lepetit, Phys. Rev. B 62 (2000) 402.
[66] N. Suaud, M.B. Lepetit, Phys. Rev. Lett. 88 (2002) 056405.

[67] W.-G. Yin, D. Volja, W. Ku, Phys. Rev. Lett. 96 (2006) 116405.
[68] B. Leuenberger, H.U. Güdel, P. Fisher, J. Solid State Chem. 64 (1986) 90.
[69] Y. Inagaki, Ph.D. Thesis, Kyushu University, Fukuoka, Japan, 2003.
[70] T. Ziman, J.P. Boucher, Y. Inagaki, Y. Ajiro, J. Phys. Soc. Jpn. 74 (Suppl.) (2005) 119–128.
[71] M.B. Stone, I. Zaliznyak, D.H. Reich, C. Broholm, Phys. Rev. B 64 (2001) 144405.
[72] B. Grenier, L.-P. Regnault, Y. Inagaki, Y. Ajiro, T. Ziman, J.-P. Boucher, Physica B 385–386 (2006) 447–449.
[73] B. Grenier, Y. Inagaki, L.P. Regnault, A. Wildes, T. Asano, Y. Ajiro, E. Lhotel, C. Paulsen, T. Ziman, J.P. Boucher, Phys. Rev. Lett. 92 (2004) 177202.
[74] B. Grenier, et al., in preparation.
[75] W.L. McMillan, Phys. Rev. B 14 (1976) 1496.
[76] S. Notbohm, P. Ribeiro, B. Lake, D.A. Tennant, K.P. Schmidt, G.S. Uhrig, C. Hess, R. Klingeler, G. Behr, B. Büchner, M. Reehuis, R.I. Bewley, C.D. Frost, P. Manuel, R.S. Eccleston, Phys. Rev. Lett. 98 (2007) 027403.
[77] K. Ohoyama, N. Katoh, H. Nojiri, Y.H. Matsuda, H. Hiraka, K. Ikeda, H.M. Shimizu, J. Phys.: Conf. Ser. 51 (2006) 506–509.
[78] L.P. Regnault, Inelastic neutron polarization analysis, in: Neutron Scattering from Magnetic Materials, Elsevier, Amsterdam, 2005 (Chapter 7).
[79] B.J. Kirby, J.A. Borchers, J.J. Rhyne, S.G.E. te Velthuis, A. Hoffmann, K.V. O'Donovan, T. Wojtowicz, X. Liu, W.L. Lim, J.K. Furdyna, Phys. Rev. B. 69 (2004) 081307(R).
[80] A. Goujon, B. Gillon, A. Debede, A. Cousson, A. Gukasov, J. Jeftic, G.J. McIntyre, F. Varret, Phys. Rev. B 73 (2006) 104413.